Differences in channel and hillslope geometry record a migrating uplift wave at the Mendocino Triple Junction

Fiona J. Clubb[1], Simon M. Mudd[2], Martin D. Hurst[3] and Stuart W. D. Grieve[4]

[1]*Department of Geography, Durham University, Lower Mountjoy, South Road, Durham, DH1 3LE, UK*

[2]*School of GeoSciences, University of Edinburgh, Drummond Street, Edinburgh, EH8 9XP, UK*

[3]*School of Geographical and Earth Sciences, University of Glasgow, Glasgow, G12 8QQ, UK*

[4]*School of Geography, Queen Mary University of London, Mile End Road, London, E1 4NS, UK*

ABSTRACT

Tectonic plate motion, and the resulting change in land surface elevation, has been shown to have a fundamental impact on landscape morphology. Changes to uplift rates can drive a response in fluvial channels, which then drives changes to hillslopes. As hillslopes respond on different timescales than fluvial channels, investigating the geometry of channels and hillslopes in concert provides novel opportunities to examine how uplift rates may have changed through time. Here we perform coupled topographic analysis of channel and hillslope geometry across a series of catchments at the Mendocino Triple Junction (MTJ) in Northern California. These catchments are characterized by an order of magnitude difference in uplift rate from north to south. We find that dimensionless hillslope relief closely matches the uplift signal across the area and is positively correlated with channel steepness. Furthermore, the range of uncertainty in hillslope relief is lower than that of channel steepness, suggesting that it may be a more reliable recorder of uplift in the MTJ region. We find that hilltop curvature lags behind relief in its

response to uplift, which in turn lags behind channel response. These combined metrics show the northwards migration of the MTJ and the corresponding uplift field from topographic data alone.

INTRODUCTION

An important challenge within Earth surface research is linking surface processes to those at depth. In the last few decades, the proliferation of topographic data has made it possible to link surface morphology and crustal processes at both higher resolutions and larger spatial scales than previously possible.

River channels, for example, adjust their morphology in response to tectonic uplift (e.g. Lavé and Avouac, 2001; Kirby et al., 2003; Duvall et al., 2004; Finnegan et al., 2005; Kirby and Whipple, 2001; 2012). A widely used metric for analyzing morphological change is normalized channel steepness (k_{sn}) which allows comparison of steepness independent of drainage area. Channel steepness, the gradient of a power-law relationship between channel slope and drainage area, has often been linked to spatial patterns of tectonic uplift (e.g. Snyder et al., 2000; Kirby et al., 2003; Wobus et al., 2006; Kirby and Whipple, 2012). Variations in k_{sn} have also been used to estimate changing uplift rates through time (e.g. Pritchard et al., 2009; Roberts and White, 2010; Goren et al., 2014; DeLong et al., 2017). However, such attempts can be complicated by additional factors affecting channel steepness, such as lithology, climate, or sediment transport.

Hillslope morphology can also serve as an important archive for crustal processes. Rivers act as the downslope boundary conditions for hillslopes (Whipple and Tucker, 1999). Therefore, tectonic signals transmitted through river networks can drive hillslope adjustment (Roering et al., 2007; Hurst et al., 2012; 2013). Large-scale studies of landscape denudation have linked relief and hillslope gradient to denudation rates (e.g. Ahnert, 1970; Harrison, 2000). However, hillslope gradient has been shown to become insensitive to denudation rates in high relief landscapes (Schmidt and Montgomery, 1995; Binnie et al., 2007, DiBiase et al., 2010). Recent advances have shown that metrics such as hilltop curvature can record signatures of erosion rates even in rapidly eroding landscapes (Roering et al., 2007; Hurst et al., 2012; Godard et al., 2016).

Investigating the coupled response of channels and hillslopes has the potential to provide constraints on how topography can archive tectonic information. In this contribution we investigate the impact of tectonic uplift rates on surface morphology near the Mendocino Triple Junction (MTJ), California. We take advantage of new techniques for extracting channel networks and drainage density (Clubb et al., 2014; 2016); channel steepness (Mudd et al., 2014; 2018); and hillslope lengths and morphologies (e.g. Hurst et al., 2012; Grieve et al., 2016a,b). We explore how combined variations in channel and hillslope morphology can be used to detect both spatial and temporal variations in uplift rates.

THE MENDOCINO TRIPLE JUNCTION

The rivers draining the northern coast of California along the San Andreas fault provide a striking example of the influence of differential rock uplift on surface morphology. We focus on 25 basins which drain to the coast and are influenced by the MTJ located offshore to the west (Fig. 1). These catchments have been the subject of extensive research due to the inferred order of magnitude difference in uplift from north to south (e.g. Merritts and Vincent, 1989; Merritts and Bull, 1989; Merritts et al., 1994; Snyder et al., 2000; 2003; Perron and Royden, 2013; Balco et al., 2013; Willenbring et al., 2013; Bennett et al., 2016; DeLong et al., 2017; Moon et al., 2018). This allows us to build upon a rich legacy of data on the channel profiles, incision patterns, erosion rates, and uplift history of the area.

Dating of marine terraces by Merritts and Bull (1989) shows that Pleistocene uplift rates along the coast vary from ~3 mm/yr in the north near the Bear River, to ~4 mm/yr at the King

Range, and then reduce to ~0.5 mm/yr further south near Fort Bragg (Fig. 1). The MTJ marks the intersection of the Juan de Fuca, Pacific, and North American plates (Furlong and Govers, 1999; Lock et al., 2006) and is migrating northwards at around 50 mm/yr (Sella et al., 2002). Therefore, the uplift signal changes latitudinally through time, such that basins to the north are in a ‘transitional zone' from low to high uplift (e.g. Snyder et al., 2000). Catchment-averaged ^{10}Be and ^{26}Al-derived erosion rates published by Moon et al. (2018) show that erosion rates broadly reflect this gradient in uplift, although are generally lower than marine terrace estimates. They found that erosion rates in the southern region are low (0.21 - 0.32 mm/yr), similar to long-term uplift rates. Catchment erosion rates in the northern transitional zone, while higher than in the south (0.43 - 0.69 mm/yr), are lower than the uplift rates estimated for the past 72 ka (3.5 - 4 mm/yr), suggesting either that catchments have not yet adjusted to the increased uplift rate, or that these uplift rates are overestimated. Work in the Santa Lucia Mountains by Young and Hilley (2018) suggested that erosion of sloping terraces may lead to higher apparent elevations and thus uplift, which may also affect estimated uplift rates in the MTJ area.

Previous work on MTJ basins has focused on how channel steepness reflects the spatial pattern of uplift. Merritts and Vincent (1989) found that gradient of the small coastal drainage basins was the most sensitive topographic parameter to uplift rate. However, their work was based on the analysis of contour maps available at the time, from which the identification of accurate channel networks is challenging (Grieve et al., 2016c). Snyder et al. (2000) used plots of channel gradient and drainage area to extract concavity (θ) and k_{sn}, and found that θ was relatively constant across the range ($\theta \approx 0.43$), whereas k_{sn} was correlated with uplift rate. Perron and Royden (2013) also extracted channel steepness using integral profile analysis on 18 of the basins, finding a similar correlation between k_{sn} and uplift rate. In contrast, less work has been done on the signature of this uplift signal outside of the river network. Bennett et al. (2016) analyzed landslide erosion rates in combination with topographic metrics in several larger basins, such as the Eel and Russian River catchments. They found that landslide erosion rates were correlated with uplift rate while hillslope gradient was invariant, suggesting that uplift in the region was therefore accommodated through increased landsliding rather than hillslope steepening.

The majority of previous studies have focused on linking topographic metrics to the spatial pattern of uplift, without considering their temporal patterns. In this contribution, we aim to investigate whether not only the spatial but also the temporal pattern of uplift can be deduced from topography alone, by analyzing channel and hillslope geometry in concert.

METHODS

We extracted a series of topographic metrics for the MTJ basins shown in Fig 1. using the USGS 10 m National Elevation Dataset (NED). We first analyzed the channel profiles by calculating θ and k_{sn} for each basin. Although k_{sn} has previously been calculated using slope-area plots (Snyder et al., 2000) and integral analysis (Perron and Royden, 2013), here we used new techniques for integral profile analysis (Mudd et al., 2014; 2018) which allow estimation of uncertainties within each basin. We found a mean concavity of $\theta = 0.42 \pm 0.13$ which we used to calculate k_{sn} in each basin (supplementary materials). We also calculated the median drainage density of each basin (D_d) by summing the total length of channels in each second order sub-basin and dividing by the drainage area. The channel network was extracted by identifying regions with positive contour curvature by combining the techniques of Pelletier (2013) and Clubb et al. (2014), as described by Grieve et al. (2016a).

The non-linear hillslope sediment flux model predicts a relationship between two metrics at steady-state, dimensionless hillslope relief R^* and erosion rate E^* (Roering et al., 2007). These metrics can be quantified by extracting hillslope gradient (S), hillslope length (L_H), and hilltop curvature (C_{HT}) from topographic data in order to compare to theoretical predictions. Variations in E^* are predominantly controlled by C_{HT}, and variations in R^* by S. We calculated S, C_{HT}, and L_H from topographic data following Hurst et al. (2012) and Grieve et al. (2016a; 2016b), and estimated the critical slope (S_c) following Hurst et al. (2019) (supplementary materials). Points with E^* and R^* values that deviate from the steady-state model may be indicative of hillslopes currently undergoing morphological adjustment (Hurst et al., 2013).

RESULTS AND DISCUSSION

Similar to the analysis of Snyder et al. (2000) and Perron and Royden (2013), we find that median k_{sn} in each basin is correlated with uplift rate (Fig. 2). We also show that variability in k_{sn} within each basin, represented by the 16th and 84th percentiles of steepness, also increases in the zone of highest uplift.

We find that R^* is elevated in the zone of highest uplift and closely mirrors the pattern of k_{sn} (Fig. 3B). However, the range in R^* between the 16th and 84th percentiles is lower than that of k_{sn}, especially in the zone of high uplift. This may be because channel profiles are generally longer than hillslopes and therefore there is more potential for noise to be recorded.

Multiple authors have described the migration of the MTJ through plate reconstructions (e.g., Atwater, 1970) or geodesy (e.g. Sella et al., 2002), but we can detect this migration recorded in hillslopes and channels by combining the metrics of k_{sn} and R^* (Fig. 3A). Basins to the south (20 - 24), which were previously uplifted, have high R^* values but low k_{sn} values: they plot above the linear fit in Fig. 3A. We suggest this is because R^* will be slower to respond to the cessation of the uplift than channel gradient. However, the northern basins (0 - 5) have lower R^* values compared to k_{sn}: they plot below the linear fit in Fig. 3A. This also suggests that channels respond more quickly to uplift: this region is in the transitional uplift zone resulting in less time for the hillslopes to steepen in response. We estimated these response timescales using independent measurements of MTJ migration. Assuming that the MTJ migrates at 50 mm/yr (Sella et al., 2002) and given that the current high uplift zone is ~70 km northwest of basins 20 - 24, we can estimate that these basins would have been in the high uplift region around 1.4 Ma. This suggests that the channel response time to decaying uplift is < 1.4 Ma, whereas the hillslope response time is > 1.4 Ma.

The northwards migration of the triple junction can also be detected by comparing E^* and R^* (Fig. 3B). Basins north of the high uplift zone (4 - 8) have elevated median R^* values but low E^* values (Fig. 2). Both basins to the north and south have low E^* values relative to basins located in the high uplift zone, but basins to the south have higher E^* and R^* values compared to the north (Fig. 3B). This pattern suggests that hillslopes and hilltops to the north have not yet responded to the increase in uplift, whereas accelerated uplift has slowed to the south and these basins are now relaxing (Hurst et al., 2013; Mudd, 2017). This signal is however less clear than that of k_{sn} and R^*, which may be due to the difficulty of constraining the critical slope parameter (S_c) or challenges in extracting C_{HT} from 10 m elevation data.

In contrast to E^* and R^*, we find that median L_H and D_d are relatively constant across the uplift field (Fig. 2). Bennett et al. (2016) found that hillslope gradient was invariant with uplift rate and suggested that hillslope response to uplift was mostly through an increase in landsliding. However our results suggest that, in basins with increased uplift rates, hillslopes are also steeper when normalized by hillslope length reflected by increasing hillslope relief (Fig. 2). The basins analyzed by Bennett et al. (2016) were much larger than the small coastal drainages upon which we focus. The basins we analyze here may contain hillslopes more representative of the current uplift rate, simply as a function of the smaller basin size, compared to the larger basins such as the Eel River. The trunk channels of these smaller basins are also oriented perpendicular to the motion of the MTJ (see Fig. 1), whereas the larger basins drain parallel to the uplift field. These larger basins are therefore less likely to be adjusted to a similar uplift rate throughout the basin.

Our results also show variability in both hillslope and channel metrics, especially in the high uplift basins (Fig 2). This may suggest that these basins are still undergoing transient adjustment. However, there are other factors that may cause spatially variable topographic metrics in the MTJ area. For example, the bedrock lithology consists of Late Cretaceous to Pliocene sandstones and mudstones (Jennings et al., 1977). Variations in rock strength or joint density may cause within-basin variability, although it has been suggested that there are no large scale discontinuities in erodibility between the catchments (Merritts and Vincent, 1989). Furthermore, complex drainage patterns in the region suggest ongoing divide migration. Performing a similar analysis on small tributaries of the Mattole River across the drainage divide (supplementary materials) shows that there is more variability in hillslope and hilltop metrics than those draining to the coast, which may complicate attempts to detect uplift signals from topography.

CONCLUSIONS

Analyzing channel profiles in combination with hillslopes can reveal spatial and temporal trends in tectonic uplift. We found that both channel steepness and hillslope relief mirror the uplift signal, constrained through independent dating of marine terraces. Despite the ubiquitous use of the channel steepness metric in tectonic geomorphology, we find that the range in hillslope relief is lower than that of channel steepness, suggesting that R^* may be a more reliable recorder of tectonics in the Mendocino Triple Junction region. Using the different response timescales of the channels, hillslopes, and hilltops, we were able to detect the northwards migration of the triple junction and uplift signal. This highlights the potential that topographic data holds, if hillslope morphology is analyzed along with that of the fluvial profile, for exploring not only the magnitude of uplift rates across the landscape, but also variation in uplift rates through time.

ACKNOWLEDGMENTS

This work was supported by a Geo.X fellowship to Clubb, and a Natural Environment Research Council grant NE/J009970/1 to Mudd. We would like to thank Georgina Bennett, George Hilley, and Liran Goren for helpful comments that significantly improved the manuscript.

REFERENCES CITED

Ahnert, F., 1970, Functional relationships between denudation, relief, and uplift in large, mid-latitude drainage basins: American Journal of Science, v. 268, p. 243–263, doi:10.2475/ajs.268.3.243.

Andrews, D.J., Bucknam, R.C., 1987, Fitting degradation of shoreline scarps by a nonlinear diffusion model: Journal of Geophysical Research: Solid Earth, v. 92, p. 12857–12867, doi: 10.1029/JB092iB12p12857.

Atwater, T., 1970, Implications of plate tectonics for the Cenozoic tectonic evolution of western North America: Geological Society of America Bulletin, v. 81, p. 3513–3536, doi: 10.1130/0016-7606(1970)81[3513:IOPTFT]2.0.CO;2.

Balco, G., Finnegan, N., Gendaszek, A., Stone, J.O.H., Thompson, N., 2013, Erosional response to northward-propagating crustal thickening in the coastal ranges of the U.S. Pacific Northwest: American Journal of Science, v. 313, p. 790–806, doi: 10.2475/11.2013.01.

Bennett, G.L., Miller, S.R., Roering, J.J., Schmidt, D.A., 2016, Landslides, threshold slopes, and the survival of relict terrain in the wake of the Mendocino Triple Junction: Geology, v. 44, p. 363–366, doi: 10.1130/G37530.1.

Binnie, S.A., Phillips, W.M., Summerfield, M.A., Fifield, L.K., 2007, Tectonic uplift, threshold hillslopes, and denudation rates in a developing mountain range: Geology, v. 35, p. 743–746, doi: 10.1130/G23641A.1.

Clubb, F.J., Mudd, S.M., Attal, M., Milodowski, D.T., Grieve, S.W.D., 2016, The relationship between drainage density, erosion rate, and hilltop curvature: Implications for sediment transport processes: Journal of Geophysical Research: Earth Surface, 2015JF003747, doi: 10.1002/2015JF003747.

Clubb, F.J., Mudd, S.M., Milodowski, D.T., Hurst, M.D., Slater, L.J., 2014, Objective extraction of channel heads from high-resolution topographic data: Water Resources Research, v. 50, p. 4283–4304, doi: 10.1002/2013WR015167.

DeLong, S.B., Hilley, G.E., Prentice, C.S., Crosby, C.J., Yokelson, I.N., 2017, Geomorphology, denudation rates, and stream channel profiles reveal patterns of mountain building adjacent to the San Andreas fault in northern California, USA: Geological Society of America Bulletin, v. 129, p. 732–749, doi: 10.1130/B31551.1.

DiBiase, R.A., Whipple, K.X., Heimsath, A.M., Ouimet, W.B., 2010, Landscape form and millennial erosion rates in the San Gabriel Mountains, CA: Earth and Planetary Science Letters, v. 289, p. 134–144, doi: 10.1016/j.epsl.2009.10.036.

Duvall, A., Kirby, E., Burbank, D., 2004, Tectonic and lithologic controls on bedrock channel profiles and processes in coastal California: Journal of Geophysical Research: Earth Surface, v. 109, F03002, doi: 10.1029/2003JF000086.

Finnegan, N.J., Roe, G., Montgomery, D.R., Hallet, B., 2005, Controls on the channel width of rivers: Implications for modeling fluvial incision of bedrock: Geology, v. 33, p. 229–232, doi: 10.1130/G21171.1.

Furlong, K.P., Govers, R., 1999, Ephemeral crustal thickening at a triple junction: The Mendocino crustal conveyor: Geology, v. 27, p. 127–130, doi: 10.1130/0091-7613(1999)027<0127:ECTAAT>2.3.CO;2.

Godard, V., Ollivier, V., Bellier, O., Miramont, C., Shabanian, E., Fleury, J., Benedetti, L., Guillou, V., 2016, Weathering-limited hillslope evolution in carbonate landscapes: Earth and Planetary Science Letters, v. 446, p. 10–20, doi: 10.1016/j.epsl.2016.04.017.

Goren, L., Fox, M., Willett, S.D., 2014, Tectonics from fluvial topography using formal linear inversion: Theory and applications to the Inyo Mountains, California: Journal of Geophysical Research: Earth Surface, v. 119, p. 1651–1681, doi: 10.1002/2014JF003079.

Grieve, Stuart W. D., Mudd, S.M., Hurst, M.D., Milodowski, D.T., 2016a, A nondimensional framework for exploring the relief structure of landscapes: Earth Surface Dynamics, v. 4, p. 309–325, doi: 10.5194/esurf-4-309-2016.

Grieve, Stuart W.D., Mudd, S.M., Hurst, M.D., 2016b, How long is a hillslope?: Earth Surface Processes and Landforms, v. 41, p. 1039–1054, doi: 10.1002/esp.3884.

Grieve, Stuart. W.D., Mudd, S. M., Milodowski, D. T., Clubb, F. J., & Furbish, D. J., 2016c, How does grid-resolution modulate the topographic expression of geomorphic processes?: Earth Surface Dynamics, v. 4, p. 627–653, doi: 10.5194/esurf-4-627-2016.

Harrison, C.G.A., 2000, What factors control mechanical erosion rates?: International Journal of Earth Sciences, v. 88, p. 752–763, doi: 10.1007/s005310050303.

Hurst, M.D., Grieve, S.W.D., Clubb, F.J., Mudd, S.M., 2019, Detection of channel-hillslope coupling along a tectonic gradient: Earth and Planetary Science Letters, v. 522, p. 30-39, doi:10.1016/j.epsl.2019.06.018.

Hurst, M.D., Mudd, S.M., Attal, M., Hilley, G., 2013, Hillslopes Record the Growth and Decay of Landscapes: Science, v. 341, p. 868–871, doi: 10.1126/science.1241791.

Hurst, M.D., Mudd, S.M., Walcott, R., Attal, M., Yoo, K., 2012, Using hilltop curvature to derive the spatial distribution of erosion rates: Journal of Geophysical Research: Earth Surface, v. 117, doi:10.1029/2011JF002057, doi: 10.1029/2011JF002057

Jennings, C.W., Strand, R.G., Rogers, T.H., 1977. Geologic map of California, scale 1:750,000. California Division of Mines and Geology, Sacramento.

Kirby, E., Whipple, K., 2001, Quantifying differential rock-uplift rates via stream profile analysis: Geology, v. 29, p. 415–418, doi: 10.1130/0091-7613(2001)029<0415:QDRURV>2.0.CO;2.

Kirby, E., Whipple, K.X., 2012, Expression of active tectonics in erosional landscapes: Journal of Structural Geology, v. 44, p. 54–75, doi: 10.1016/j.jsg.2012.07.009.

Kirby, E., Whipple, K.X., Tang, W., Chen, Z., 2003, Distribution of active rock uplift along the eastern margin of the Tibetan Plateau: Inferences from bedrock channel longitudinal profiles: Journal of Geophysical Research: Solid Earth, v. 108, p. 2217, doi: 10.1029/2001JB000861.

Lavé, J., Avouac, J.P., 2001, Fluvial incision and tectonic uplift across the Himalayas of central Nepal: Journal of Geophysical Research: Solid Earth, v. 106, p. 26561–26591, doi: 10.1029/2001JB000359.

Lock, J., Kelsey, H., Furlong, K., Woolace, A., 2006, Late Neogene and Quaternary landscape evolution of the northern California Coast Ranges: Evidence for Mendocino triple junction tectonics: GSA Bulletin, v. 118, p. 1232–1246, doi: 10.1130/B25885.1.

Merritts, D., Bull, W.B., 1989, Interpreting Quaternary uplift rates at the Mendocino triple junction, northern California, from uplifted marine terraces: Geology, v. 17, p. 1020–1024, doi: 10.1130/0091-7613(1989)017<1020:IQURAT>2.3.CO;2.

Merritts, D., Vincent, K.R., 1989, Geomorphic response of coastal streams to low, intermediate, and high rates of uplift, Mendocino triple junction region, northern California: GSA Bulletin, v. 101, p. 1373–1388, doi: 10.1130/0016-7606(1989)101<1373:GROCST>2.3.CO;2.

Merritts, D.J., Vincent, K.R., Wohl, E.E., 1994, Long river profiles, tectonism, and eustasy: A guide to interpreting fluvial terraces: Journal of Geophysical Research: Solid Earth, v. 99, p. 14031–14050, doi: 10.1029/94JB00857.

Moon, S., Merritts, D.J., Snyder, N.P., Bierman, P., Sanquini, A., Fosdick, J.C., Hilley, G.E., 2018, Erosion of coastal drainages in the Mendocino Triple Junction region (MTJ), northern California: Earth and Planetary Science Letters, v. 502, p. 156–165, doi: 10.1016/j.epsl.2018.09.006.

Mudd, S.M., 2017, Detection of transience in eroding landscapes: Earth Surface Processes and Landforms, v. 42, p. 24–41, doi: 10.1002/esp.3923.

Mudd, S.M., Attal, M., Milodowski, D.T., Grieve, S.W.D., Valters, D.A., 2014, A statistical framework to quantify spatial variation in channel gradients using the integral method of channel profile analysis: Journal of Geophysical Research: Earth Surface, v. 119, p. 138–152, doi: 10.1002/2013JF002981.

Mudd, S.M., Clubb, F.J., Gailleton, B., Hurst, M.D., 2018, How concave are river channels?: Earth Surface Dynamics, v. 6, p. 505–523, doi: 10.5194/esurf-6-505-2018.

Pelletier, J.D., 2013, A robust, two-parameter method for the extraction of drainage networks from high-resolution digital elevation models (DEMs): Evaluation using synthetic and real-world DEMs: Water Resources Research, v. 49, p. 75–89, doi: 10.1029/2012WR012452.

Perron, J.T., Royden, L., 2013, An integral approach to bedrock river profile analysis: Earth Surface Processes and Landforms, v. 38, p. 570–576, doi: 10.1002/esp.3302.

Pritchard, D., Roberts, G.G., White, N.J., Richardson, C.N., 2009, Uplift histories from river profiles: Geophysical Research Letters, v. 36, doi: 10.1029/2009GL040928.

Roberts, G.G., White, N., 2010, Estimating uplift rate histories from river profiles using African examples: Journal of Geophysical Research: Solid Earth, v. 115, B02406, doi: 10.1029/2009JB006692.

Roering, J.J., Kirchner, J.W., Dietrich, W.E., 1999, Evidence for nonlinear, diffusive sediment transport on hillslopes and implications for landscape morphology: Water Resources Research, v. 35, p. 853–870, doi: 10.1029/1998WR900090.

Roering, J.J., Perron, J.T., Kirchner, J.W., 2007, Functional relationships between denudation and hillslope form and relief: Earth and Planetary Science Letters, v. 264, p. 245–258, doi: 10.1016/j.epsl.2007.09.035.

Schmidt, K.M., Montgomery, D.R., 1995, Limits to Relief: Science, v. 270, p. 617–620, doi: 10.1126/science.270.5236.617.

Sella, G.F., Dixon, T.H., Mao, A., 2002, REVEL: A model for Recent plate velocities from space geodesy: Journal of Geophysical Research: Solid Earth, v. 107, ETG 11-1, doi: 10.1029/2000JB000033.

Snyder, N.P., Whipple, K.X., Tucker, G.E., Merritts, D.J., 2003, Channel response to tectonic forcing: field analysis of stream morphology and hydrology in the Mendocino triple junction region, northern California: Geomorphology, v. 53, p. 97–127, doi: 10.1016/S0169-555X(02)00349-5.

Snyder, N.P., Whipple, K.X., Tucker, G.E., Merritts, D.J., 2000, Landscape response to tectonic forcing: Digital elevation model analysis of stream profiles in the Mendocino triple junction region, northern California: Geological Society of America Bulletin v. 112, p. 1250–1263, doi: 10.1130/0016-7606(2000)112<1250:LRTTFD>2.0.CO;2.

Whipple, K.X., Tucker, G.E., 1999, Dynamics of the stream-power river incision model: Implications for height limits of mountain ranges, landscape response timescales, and research needs: Journal of Geophysical Research: Solid Earth, v. 104, p. 17661–17674, doi: 10.1029/1999JB900120.

Willenbring, J.K., Gasparini, N.M., Crosby, B.T., Brocard, G., 2013, What does a mean mean? The temporal evolution of detrital cosmogenic denudation rates in a transient landscape: Geology, v. 41, p. 1215–1218, doi: 10.1130/G34746.1.

Wobus, C., Whipple, K.X., Kirby, E., Snyder, N., Johnson, J., Spyropolou, K., Crosby, B., Sheehan, D., 2006, Tectonics from topography: Procedures, promise, and pitfalls:

Geological Society of America Special Papers, v. 398, p. 55–74, doi: 10.1130/2006.2398(04).
Young, H.H., Hilley, G.E., 2018, Millennial-scale denudation rates of the Santa Lucia Mountains, California: Implications for landscape evolution in steep, high-relief, coastal mountain ranges: GSA Bulletin, v. 130, p. 1809-1824, doi: 10.1130/B31907.1.

FIGURE CAPTIONS

Figure 1. Shaded relief map of the study area, showing the 25 basins draining the Californian coast next to the Mendocino Triple Junction. Basins are colored by distance southwards from the Bear River, the most northerly basin. The inset map shows the location of the field site within California.

Figure 2. Median hillslope and channel data for the 25 basins, showing variation in hillslope length (L_H), dimensionless erosion rate (E^*), dimensionless relief (R^*), normalized channel steepness (k_{sn}), and drainage density (D_d). The gray bars represent the 16th and 84th percentiles of the distributions within each basin. The bottom panel shows the Pleistocene uplift rates calculated by Merritts and Bull (1989).

Figure 3. (A) Scatter plot of normalized channel steepness (k_{sn}) against R^* for the 25 basins. The points are colored by the basin key (red colors indicate northerly and blue colors southerly basins). The dashed line represents a linear fit through the data, with $R^2 = 0.81$ and $p < 0.01$. Arrows represent movement of a basin through R^*-k_{sn} space during the passage of a transient uplift wave. (B) Plot of R^* vs. E^* for the 25 basins, coloring same as in (A). The dashed line

represents the steady state relationship between E^* and R^* predicted by Roering et al. (2007). The critical slope value, S_c, is set to 0.8. Arrows represent movement of a basin through E^*-R^* space during the passage of a transient uplift wave.

[Please include this text at the end of your paper if you are including an item in the Data Repostitory.]

[1]GSA Data Repository item 201Xxxx, additional methodological details and supporting figures for the topographic analysis, and tables with the calculated topographic data for each basin, is available online at www.geosociety.org/pubs/ft20XX.htm, or on request from editing@geosociety.org or Documents Secretary, GSA, P.O. Box 9140, Boulder, CO 80301, USA.

Figure 1

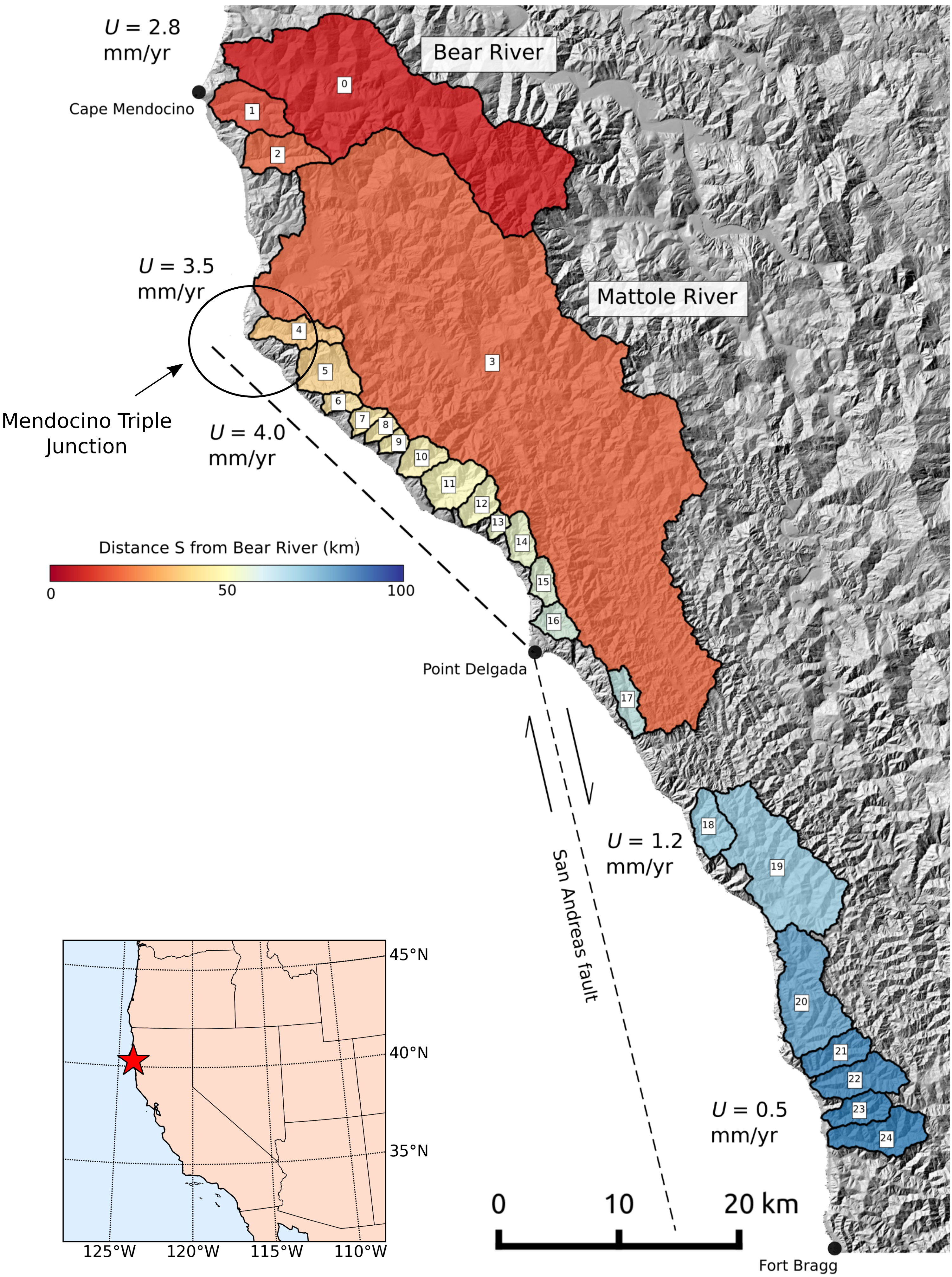

U = 2.8 mm/yr
Cape Mendocino
Bear River
U = 3.5 mm/yr
Mattole River
Mendocino Triple Junction
U = 4.0 mm/yr
Distance S from Bear River (km)
0
50
100
Point Delgada
U = 1.2 mm/yr
San Andreas fault
U = 0.5 mm/yr
0
10
20 km
Fort Bragg
45°N
40°N
35°N
125°W
120°W
115°W
110°W

Figure 2

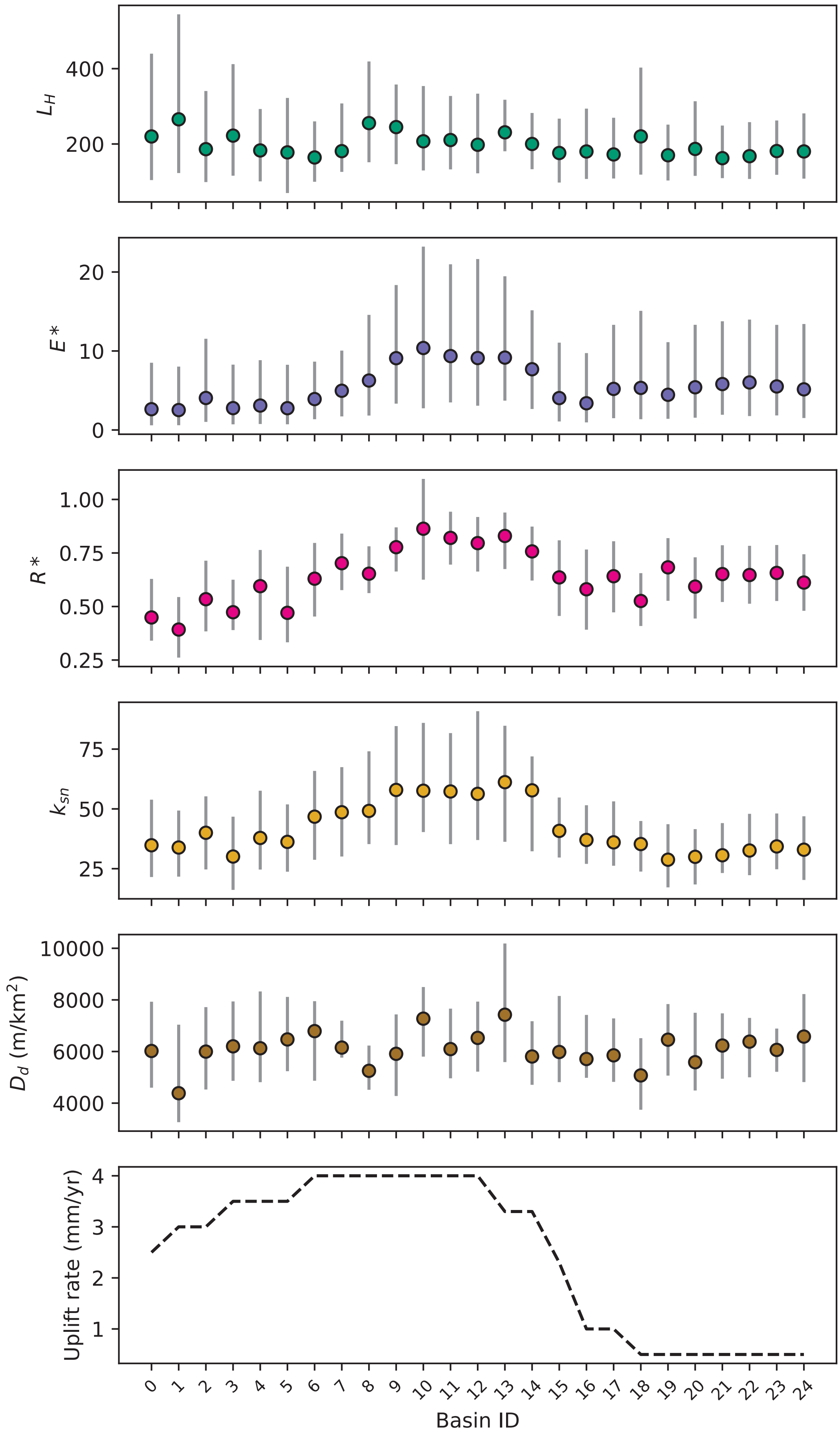

L_H
200
400
$E*$
0
10
20
$R*$
0.25
0.50
0.75
1.00
k_{sn}
25
50
75
D_d (m/km^2)
4000
6000
8000
10000
Uplift rate (mm/yr)
1
2
3
4
0 1 2 3 4 5 6 7 8 9 10 11 12 13 14 15 16 17 18 19 20 21 22 23 24
Basin ID

Figure 3

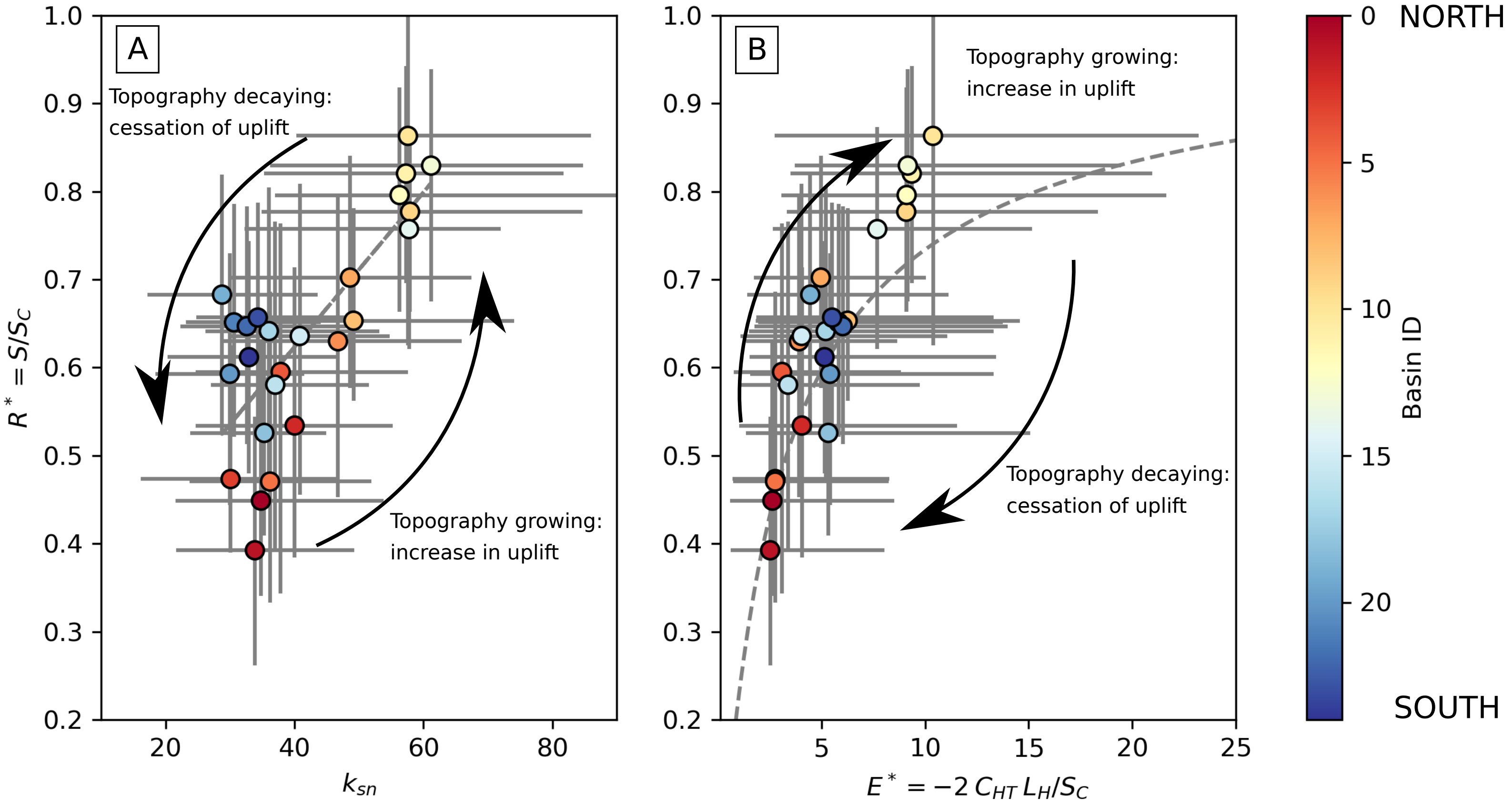

A
Topography decaying:
cessation of uplift
Topography growing:
increase in uplift
$R^* = S/S_C$
k_{sn}
1.0
0.9
0.8
0.7
0.6
0.5
0.4
0.3
0.2
20
40
60
80
B
Topography growing:
increase in uplift
Topography decaying:
cessation of uplift
$E^* = -2\, C_{HT}\, L_H/S_C$
5
10
15
20
25
0
NORTH
SOUTH
Basin ID